ORIGINAL RESEARCH

The therapeutic effect and MR molecular imaging of FA-PEG-FePt/DDP nanoliposomes in AMF on ovarian cancer

Xuefeng Bian [iD][1],*, Ting Guo[2],*, Guojie Chen[2],*, Dengyun Nie[2], Miao Yue [iD][2], Yinxing Zhu[2], Mei Lin[3]

[1]Imaging Department, The Affiliated Taizhou People's Hospital of Nanjing Medical University, Taizhou School of Clinical Medicine, Nanjing Medical University, Taizhou, People's Republic of China; [2]Institute of Clinical Medicine, The Affiliated Taizhou People's Hospital of Nanjing Medical University, Taizhou School of Clinical Medicine, Nanjing Medical University, Taizhou, People's Republic of China; [3]Clinical Medical Laboratory, The Affiliated Taizhou People's Hospital of Nanjing Medical University, Taizhou School of Clinical Medicine, Nanjing Medical University, Taizhou, People's Republic of China

*These authors contributed equally to this work

Correspondence: Mei Lin; Yinxing Zhu, Email trylm@ntu.edu.cn; lzp_zyx@163.com

Purpose: This study aimed to construct targeting drug-loading nanocomposites (FA-FePt/DDP nanoliposomes) to explore their potential in ovarian cancer therapy and molecular magnetic resonance imaging (MMRI).

Methods: FA-FePt-NPs were prepared by coupling folate (FA) with polyethylene-glycol (PEG)-coated ferroplatinum nanoparticles and characterized. Then cisplatin (DDP) was encapsulated in FA-FePt-NPs to synthesize FA-PEG-FePt/DDP nanoliposomes by thin film-ultrasonic method and high-speed stirring, of which MMRI potential, magnetothermal effect, and the other involved performance were analyzed. The therapeutic effect of FA-FePt/DDP nanoliposomes combined with magnetic fluid hyperthermia (MFH) on ovarian cancer in vitro and in vivo was evaluated. The expression levels of Bax and epithelial–mesenchymal transition related proteins were detected. The biosafety was also preliminarily observed.

Results: The average diameter of FA-FePt-NPs was about 30 nm, FA-FePt/DDP nanoliposomes were about 70 nm in hydrated particle size, with drug slow-release and good cell-specific targeted uptake. In an alternating magnetic field (AMF), FA-FePt/DDP nanoliposomes could rapidly reach the ideal tumor hyperthermia temperature (42~44 °C). MRI scan showed that FA-FePt-NPs and FA-FePt/DDP nanoliposomes both could suppress the T2 signal, indicating a good potential for MMRI. The in vitro and in vivo experiments showed that FA-FePt/DDP-NPs in AMF could effectively inhibit the growth of ovarian cancer by inhibiting cancer cell proliferation, invasion, and migration, and inducing cancer cell apoptosis, much better than that of the other individual therapies; molecularly, E-cadherin and Bax proteins in ovarian cancer cells and tissues were significantly increased, while N-cadherin, Vimentin, and Bcl-2 proteins were inhibited, effectively inhibiting the malignant progression of ovarian cancer. In addition, no significant pathological injury and dysfunction was observed in major visceras.

Conclusion: We successfully synthesized FA-FePt/DDP nanoliposomes and confirmed their good thermochemotherapeutic effect in AMF and MMRI potential on ovarian cancer, with no obvious side effects, providing a favorable strategy of integrated targeting therapy and diagnosis for ovarian cancer.

Keywords: iron–platinum magnetic nanoparticles, ovarian cancer, DDP, molecular magnetic resonance imaging, folate

Introduction

As one of the common tumors in the female reproductive system, ovarian cancer lists first among gynecological tumors in mortality.[1] Although considerable progress has been made, the diagnosis and therapy of ovarian cancer are not satisfactory. Up to the present, the pathological examination remains the gold standard for the diagnosis of ovarian cancer; however, the process is invasive and it is difficult to detect the tumor tissue in non-surgery.[2] Surgery combined with chemotherapy is considered the routine method for the treatment of ovarian cancer,[3] but most patients are at

advanced stage and lose the best chance of surgery because of ovarian cancer concealment. Concurrently, most of the current medications are administered intravenously and have non-selectivity of cancer tissue. As a result, it is difficult for the anti-tumor medicine to maintain high concentration in the lesion location, leading to poor efficacy and severe side effects.[4,5] Therefore, it is in great demand to seek a non-invasive, safe, sensitive, and accurate diagnosis method and effective therapy with less adverse effects for ovarian cancer.

Magnetic resonance imaging (MRI), an extensively applied non-invasive medical diagnostic technology at present, has unique advantages in the diagnosis of various tumors, such as liver cancer, cervical cancer, ovarian cancer, glioma, and other tumors, due to its high pixel and good soft tissue contrast,[6] and can qualitatively distinguish malignant tumors from normal tissues. However, conventional MRI shows poor sensitivity to the tiny lesions, and as a result it is not suitable for the early diagnosis of ovarian cancer. Inspiringly, considerable great progress has been made in molecular imaging, especially in molecular MRI in recent years. Owing to excellent magnetism property, magnetic nanomaterials including ferric oxide[7–9] and metal alloy[10–14] have been used as agents to strengthen MRI. Bimetallic or trimetallic nanoparticles are more effective than monometallic nanoparticles due to their excellent synergistic properties and stable structures.[15] After modified with specific antibody, ligand, magnetic nanomaterials may be used for molecular magnetic resonance imaging (MMRI) or other molecular probes.[16] Theoretically, MMRI may well improve the sensitivity of MRI and thus promote the detection of early cancer, but they are almost still in the laboratory research stage, rarely applied in clinic.

With the exception of MRI contrast agent or molecular probe, magnetic nanomaterials can be used as drug carriers after being modified with specific antibody, aptamer, or peptide, etc. to conduct targeting therapy in cancer.[17] Moreover, because of good magnetothermal effect, magnetic nanomaterials also can be used for cancer thermotherapy. As one of bimetallic magnetic nanomaterials, FePt nanoparticles have attracted much attention in the biomedical field. They can increase the dose of external radiation absorbed by tumors by absorbing high amounts of X-rays.[18] Yanhong Zheng et al[19] studied in vitro MRI and CT scanning and reported the application prospect of FePt nanoparticles as dual-mode contrast agents in MRI/CT molecular imaging. It was reported that the chemotherapy drugs encapsulated in FePt nanoparticles could slowly release; the effective synergistic effect of magnetothermal and chemotherapy was achieved, thus significantly killing tumor cells at very low doses.[20]

As an alternative treatment for cancer, thermotherapy can not only directly kill tumor cells through heat energy, but also enhance the sensitivity of radiotherapy, chemotherapy, and immunotherapy, and reduce drug resistance, playing a complementary synergistic effect. Studies have shown that heating at 42 °C for 30 minutes can increase the toxicity of cisplatin and other chemotherapy drugs by 30 times, and can double the killing ability of chemotherapeutics with weak cytotoxicity at room temperature after heating.[21] However, it is difficult to evenly heat tumor tissue at a desired temperature, without damage to adjacent normal tissue.

Encouragingly, magnetic fluid hyperthermia (MFH) invented in recent years can well control the temperature to exert cancer thermotherapy. Magnetic fluid is a kind of liquid magnetic nanoparticle (MNP), which has both the fluidity of liquid and the magnetism of solid magnetic materials. When placed in an alternating magnetic field (AMF), MNPs can convert magnetic energy into heat, steadily increase the temperature of local tumor tissue, and thus play a role in killing tumor cells or inhibiting tumor growth.[22] More significantly, only can the temperature of tumor tissues and cells with MNPs rise because of magnetothermal effect; it is thus also called intracellular hyperthermia.

Cisplatin (DDP), one of the most applied chemotherapeutic agents in the clinic, exhibits good therapeutic efficacy for lung, prostate, thyroid, and ovarian cancer. However, DDP is mainly administered through intravenous methods in the clinic. Due to no selectivity to tumor tissue, the concentration of DDP in the plasma of patients rapidly rises after administration, which causes serious adverse reaction including gastrointestinal symptoms (eg decreased appetite, nausea, vomiting, diarrhea), myelosuppression, allergic reactions, neurotoxicity, and renal toxicity, even kidney failure or death.[23] The increasing prevalence of drug resistance resulting from the singular application of DDP chemotherapy has emerged as a significant concern in recent years. Consequently, it should be taken into consideration to improve in DDP targeting, dosage form and persistent release and drug resistance.

FR-α (Folate receptor alpha), a glycoprotein anchored to the cell membrane by glycosylated phosphatidylinositol (GPI), is one member of the folate receptor (FR) family with a molecular weight of 38 kDa. It has high affinity to folate

(FA) and can transport FA by receptor-mediated endocytosis. In most malignant tumors originating from epithelium, particularly in ovarian cancer, FR-α is overexpressed and the FR-α level was positively correlated with tumor differentiation and pathological grade,[24,25] whereas low expressed in normal tissues.[26] In this regard, FR-α may represent a good molecular marker for ovarian cancer diagnosis and prognosis evaluation.[27] In recent years, anti-ovarian cancer therapy and diagnosis studies based on FR-α have been widely conducted in preclinical or clinical studies.[28] FA is a small molecule vitamin with good stability. Owing to high affinity to FR-α, small molecular weight, and low immunogenicity, it is popularly used as a "biological missile" for molecular imaging or targeting therapy of tumor with FR-α.

The present study focused on constructing molecular probe FA-FePt-NPs through integrating FePt-NPs and FA to conduct MMRI for ovarian cancer diagnosis. Then, using FA-FePt-NPs as a drug carrier, DDP was loaded to construct FA-FePt/DDP-NPs to get an integration of targeted thermo-chemotherapy and diagnosis for ovarian cancer. In detail, during intervening ovarian cancer in AMF, FePt-NPs could conduct hyperthermia because of their good magnetocaloric effect while DDP is released to exert chemotherapy, resulting in a targeted thermo-chemotherapy guided by FA on ovarian cancer with FR overexpressed; in the meantime, the therapy effect could be dynamically monitored by MMRI. In short, we conducted MMRI for ovarian cancer diagnosis and thermo-chemotherapy by FA-FePt/DDP-NPs in AMF, and shed novel lights on a potential strategy to together diagnose and treat ovarian cancer and other tumors with overexpressed FR (Scheme 1).

Materials and Methods

Cell Lines and Reagents

HO8910 (human ovarian cancer cells), HeLa (human cervical cancer cells), and L-929 (fibroblast normal cell line) were purchased from Shanghai Institute of Cell Science, Chinese Academy of Sciences (Shanghai, China), along with
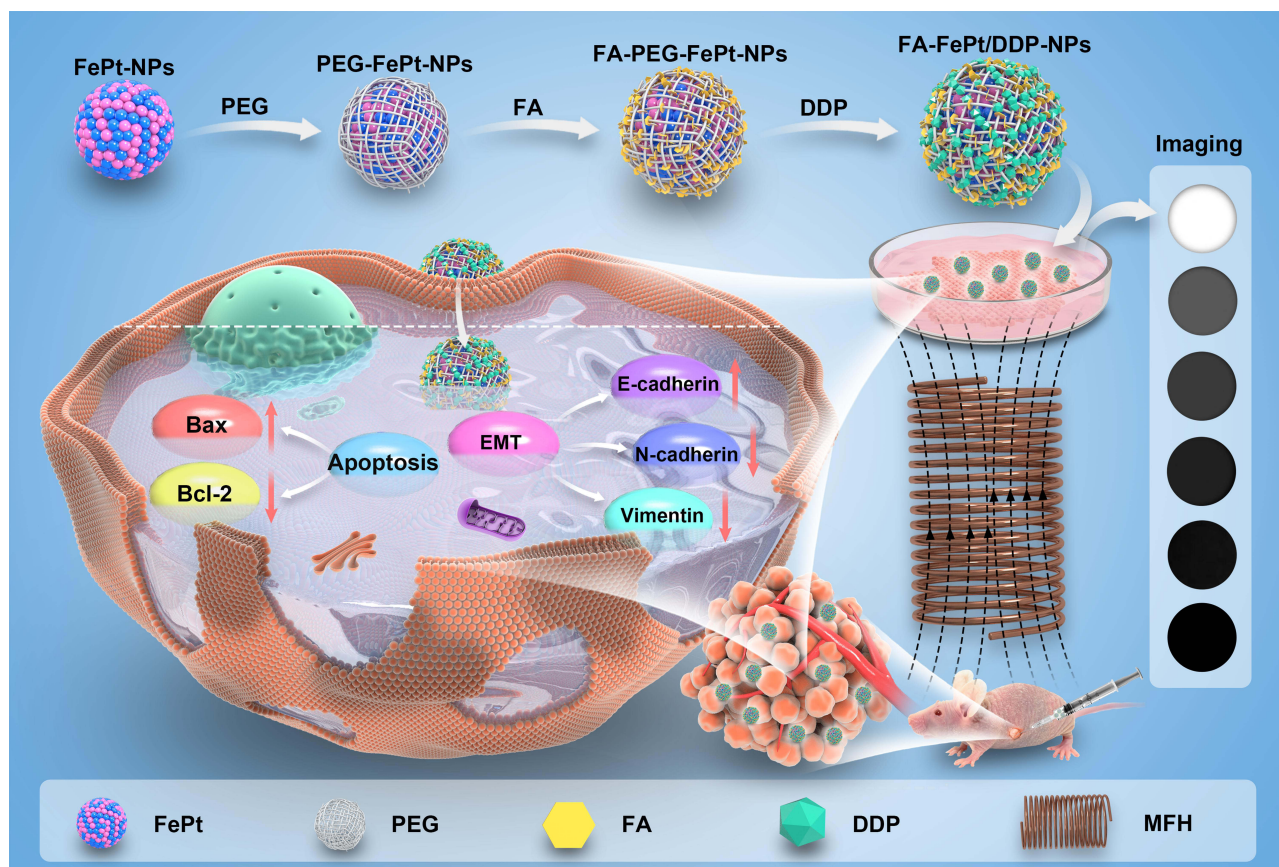
Scheme 1 Schematic illustrating the construction of FA-PEG-FePt/DDP nanoliposomes, the treatment of ovarian cancer, and magnetic resonance molecular imaging.

polyethylene glycol (PEG) (Sigma, USA), oleic acid (Chinese, medicine), MTT (Shanghai, Shenggong), IMEM medium (Gibco, USA), FBS (Gibco, USA), DMSO (Sigma, USA), PCR expansion additive kit (Shanghai Shenggong), Cisplatinum (Haosoh Pharma, Jiangsu), resistance to FA-α antibodies (Abcam, Shanghai), Annexin V-FITC Apoptosis Kit (BD, USA), and propidium iodide (PI) (Invitrogen). Morphology was characterized by a Tecnai G2 spirit BioTwin transmission electron microscope.

The Preparation of PEG-FePt-NPs

Oleic acid-coated ferro platinum magnetic nanoparticles (FePt-NPs) were prepared by a high-temperature liquid-phase reduction method according to the reference.[29] In detail, 60 mg DSPE-PEG 2000 powder was dissolved in 5 mL trichloromethane, and 3 mL FePt-NPs (the concentration was 5 mg Fe/mL and dispersed in chloroform) were removed. Then the two were mixed into a round-bottom flask. After fully ultrasonic at 70 °C for 10 min, 5 mL deionized water was added and mixed well. The round-bottom flask was put on a rotary evaporator with water bath at 70 °C, then pumped to vacuum and rotate evaporation. When the organic solvent evaporated out, the nanomaterial was transformed from an oil phase to an aqueous phase. Then the nanomaterial was cooled to room temperature, and sonicated for 15 min to disperse. The bottom sediment was removed after precipitation, and the upper solution was taken out and stored in a refrigerator at 4 °C.

Examination of the Physicochemical Properties and the Biocompatibility of PEG-FePt-NPs

The FePt-NPs and PEG-FePt-NPs were dispersed in absolute ethanol by ultrasonic method and observed by a transmission electron microscope (TEM; TecnaiG20, FEI, USA). The changes of the surface functional groups of FePt-NPs before and after modification was analyzed by a Fourier transform infrared spectroscopy (HYPERION, Bruker, Germany). X-ray diffraction (XRD) was used to analyze the characteristic peaks of the samples. Energy dispersive X-ray (EDX) was applied to detected the elements and the composition of the samples. The flat-bottomed test tubes with PEG-FePt-NPs magnetic fluid (0.25, 0.5, 1.0 and 1.5 mg/mL) were placed in AMF (225 kHz, 4 kW, 40 A) using SPG-10(A)-11 (Shuangping Power, Shenzhen, China), and the temperature of the magnetic fluid in each tube was recorded at different time within one hour. PEG-FePt-NPs solution (1 mg/mL) was diluted in IMEM culture medium, and L-929 cells were cultured in 96-well plates (5×10^4 cells/well) and intervened with PEG-FePt-NPs at 1 mg/mL, 0.5 mg/mL and 0.25 mg/mL. The positive control group was treated with 0.7% acrylamide solution. After incubation at 12 h, 24 h and 36 h, 20 μL MTT was added to each well and continued to incubate for 4 h, then 150 μL DMSO was added and fully mixed. The OD value of each well was detected at 490 nm wavelength. The formula of cell proliferation rate (RGR) was RGR%=(OD value of the experimental group/OD value of the control group)×100%. According to Table 1, the RGR values are categorized into a 5-level response scale.[30] The experimental results in the response level of 0–1 mean no cytotoxicity, and grade 2 needs to be further evaluated according to cell morphology. The results in the 3–5 range are considered cytotoxic.

Preparation and Characterization of FA-FePt-NPs Molecular Probe

PEG-FePt-NPs (1 mg/mL) were dissolved in 0.02 mol/L MES buffer and shaken well, then 2 mg EDC solid powder and 2 mg NGS solid powder were added, fully dissolved and shaken for 25 min using a shaker to ensure the full activation of –COOH on the PEG-FePt-NPs surface, and then were ultracentrifuged (Sorvall ST16R, Thermo Fisher, USA) and washed by deionized water. FA was added to the mixture and incubated at room temperature for 24 h on a shaking table. After ultrafiltration and centrifugation, FA-PEG-FePt-NPs were obtained and stored at 4 °C. The surface functional groups of PEG-FePt-NPs before and after modification were examined

Table 1 Relative Proliferation Rate and Toxicity Classification Conversion Table

Toxic reaction	0	1	2	3	4	5
RGR (%)	>100	75–99	50–74	25–49	1–24	0

by a Fourier transform infrared spectroscopy (HYPERION, Bruker, Germany) to verify the coupling of FA with PEG-FePt-NPs.

Preparation and Characterization of FA-PEG-FePt/DDP Nanoliposomes

FA-PEG-FePt/DDP nanoliposomes (FA-FePt/DDP-NPs) were prepared by thin film-ultrasonic method and high-speed stirring as follows.[31] To be specific, 40 mg DSPC, 20 mg cholesterol, 2 mg magnetic phospholipid, and the other substances were dissolved in 10 mL chloroform. After ultrasonic dispersion, the organic solvent was removed by rotary evaporation, and 4 mg DDP was dissolved and then evaporated again to form a thin film organic solvent. After freeze drying, the organic solvent was removed, and then 10 mL deionized water was added and rotated in a 45 °C water bath. Finally, FA-PEG-FePt-NPs in aqueous phase were added, and FA-FePt/DDP-NPs were obtained after 10 min treatment with ultrasonic probe. The morphology of the synthesized nanoparticles was observed by TEM (TecnaiG20, FEI, USA); the hydrodynamic size was measured by dynamic light scattering (DLS); the zeta potential was detected by a zeta potential analyzer (Colloidal Dynamics, USA); magnetic behavior was checked by vibrating sample magnetometry (Lake Shore, USA); and the size of FA-FePt/DDP-NPs at room temperature was detected by DLS every 20 h until 140 h to evaluate FA-FePt/DDP-NPs' stability in size.

The Hemolytic Test of PEG-FePt-NPs and FA-PEG-FePt-NPs

Ffresh anticoagulant blood (4 mL) obtained from healthy volunteers from the Clinical Medical Laboratory of Taizhou People's Hospital (approved by the Ethics Committee of Taizhou People's Hospital and informed consent of blood donors) was diluted in 8 mL normal saline. Then 10 mL PEG-FePt-NPs (Fe: 1 mg/mL) and 10 mL FA-PEG-FePt-NPs (Fe: 1 mg/mL) were diluted with normal saline, respectively. Also, 10 mL normal saline was used as negative control and 10 mL distilled water as positive control. Three parallel test tubes were set in each group and 0.2 mL of the diluted fresh anticoagulant blood was added to each tube. After a 37 °C water bath for 15 min, the OD value of the supernatant in each group was measured at 545 nm using Synergy HT (BioTek, USA). The hemolysis rate (%) was calculated using the formula: hemolysis rate (%)=(mean OD of the sample–mean OD of the negative control group)/(mean OD of the negative control group)×100%.

Cell Uptake Assay

HO8910 cells were inoculated into 12-well plates at a density of 1×10^5 cells per well, and then intervened with FA-FePt /DDP-NPs, while the cells without FA-FePt/DDP-NPs were used as control. After intervention for 2, 6 and 12 h, the cells were washed twice with PBS, and then were resuspended in PBS. Then 400 μL of cell suspension was collected, and the fluorescence intensity of the cells was detected by the DiD-labelled FA-FePt/DDP-NPs at different times.

In vitro MRI Analysis of PEG-FePt-NPs, FA-PEG-FePt-NPs, and FA-PEG-FePt/DDP Nanoliposomes

Sterilized FA-PEG-FePt-NPs and PEG-FePt-NPs (0.2 mg/mL) solution was added to ovarian cancer cells (HO8910) (FR-α^+) and cervical cancer (HeLa) cells (FR-α^-) respectively. Incubated for 1 hour later, the cells were washed twice with PBS and fixed in a 2.5% glutaraldehyde solution, while untreated cells were used as controls. Each group was scanned by SIEMENS Verio 3.0 TMR and its T2 signal suppression was observed, respectively. PEG-FePt-NPs and FA-FePt/DDP-NPs with the concentration of 0.025, 0.05, 0.1, 0.2, and 0.4 mg/mL were placed in the corresponding Eppendorf tube before agar-cooling and imaged by SIEMENS Verio 3.0 TMR, respectively. The axial FES T2WI sequence scanning parameters were set as TR 5000 ms, TE 146.80 ms, layer thickness 3 mm, layer spacing 1 mm, FOV 160 mm×160 mm, matrix 256×256. After scanning, the T2 value of each image was measured to calculate the relaxation rate of each sample.

In vitro Intervention of Ovarian Cancer Cells by FA-PEG-FePt/DDP Nanoliposomes in AMF

Ovarian cancer HO8910 cells at logarithmic growth stage were inoculated into 96-well plates at a density of 5×10^4 cells/well and 6-well plates (2×10^5 cells/well), and the groups were grouped as (A) negative control group (normal saline), (B) DDP group, (C) PEG-FePt-NPs/MFH group, (D) FA-FePt-NPs/MFH group, (E) FA-FePt/DDP-NPs/MFH group, and intervened with corresponding experimental agents. Group C, D, and E were placed on the plate coil of SPG-10A-II high frequency magnetic induction heater (Shuangping Power, Shenzhen, China) with a frequency of 215 kHz, rated power of 2.4 kW and output current of 40 A for 1 h, and then all the groups were routinely cultured in cell incubator for 24 h.

Cell Proliferation Inhibition Assay

After 96-well plates of each group continued to be routinely cultured until 48 h, 20 μL MTT was added to each well, continuing to incubate for 4 h, then 150 μL DMSO was added to each well and oscillated for 10 min. OD values were read using the microplate reader (Synergy HT, BioTek, USA) at the wavelength of 490 nm. Inhibition rate of cell proliferation (%)=(1 - OD of the experimental group/OD of the negative control group)×100%.

Cell Apoptosis Assay

The cells in 6-well plates of each group intervened for 24 h were digested and collected, respectively, and washed twice with PBS, then the staining binding buffer was added to resuspend the cells, and 100 μL cell suspension of each group was taken into the corresponding EP tube. After mixing with 5 μL Annexin-V–fluorescein isothiocyanate (Annexin V) and 2.5 μL propidium iodide (PI) and incubated at room temperature for 15 min away from light, 400 μL PBS were added and mixed. Subsequently, cell apoptosis was detected by FACS Aria Sorter flow cytometer (Becton Dickinson, San Jose, USA).

Wound Healing Assay

The cell concentration was adjusted to 2×10^5 cells/well and inoculated into the 6-well plate. The grouping and intervention were the same as the above. The wound was marked by a 10 μL plastic tip. The scratch width was observed by an inverted microscope at 0 h and 24 h. The blank area of the scratch was calculated by Image J software, and the wound healing rate (%)=(1–S 24 h/S 0 h)×100%.

Cell Migration and Invasion Assays

Cell invasion was analyzed using transwell chambers pre-treated Matrigel (8 μm pore; Millipore, Billerica, USA), while the migration assay was conducted in chambers without Matrigel. After treated as the above, 200 μL cell suspension (4×10^5 cells/well) of each group was prepared using serum-free medium and added to the upper chambers. The lower chambers were filled with the complete medium as chemoattractant. After incubated for 24 h, the cells were stained with 0.1% crystal violet for 20 min and then observed using a light microscope (NikonTi2, Japan).

Western Blot

After intervention as the above, total protein of each group was extracted and the concentration was detected using a BCA Kit (Thermo Fisher Scientific). Then the protein of each group was separated using 10% SDS-PAGE and transferred to PVDF membranes (Millipore). After blocking by 5% skim milk, the membranes were incubated with anti-E-cadherin, anti-N-cadherin, anti-Vimentin, anti-Bax, anti-Bcl-2, and anti-GAPDH (Abcam) antibodies at 4 °C overnight. Next, the membranes were incubated with HRP conjugated goat anti-rabbit (Abcam, Cambridge, USA) at room temperature for 1 h. After visualizing the ECL substrate (Thermo Fisher Scientific), the membranes were placed in a gel imaging system (BOX Chemi XRQ) for imaging. The expression of proteins was analyzed by ImageJ software.

Efficacy of FA-PEG-FePt/DDP Nanoliposomes in vivo

All animal experiments were approved by the Animal Management and Use Committee of China Medical City Safety Evaluation Center (Taizhou, China) in accordance with the Basel Declaration and in conformity with the Guide for the Care and Use of Laboratory Animals (National Academies Press, 2011), approval number: IACUC-2022-0009. Six-week-old female BALB/C mice, 20–22 g in weight, were purchased from Huachuang Cino Medical Technology Co., Ltd (Jiangsu Province, China) and maintained in an SPF environment. Ovarian cancer H08910 cells (5×10^5) were injected into the armpit of mice to establish a mouse ovarian cancer xenograft tumor model, and the mice were randomly divided into five groups as the same with in vitro experiment. DDP (3 mg/kg), PEG-FePt-NPs (2 mL/kg), and FA-FePt-NPs or FA-FePt/DDP-NPs (2 mL/kg) were injected into the tumors of each group by multi-point injection (above, below, left, and right), respectively. Then the mice of the groups involved in MFH were exposed to an alternating magnetic field of 2.4 kW and 215 kHz for 30 min, and the tumor temperature was recorded with an infrared thermal imager (HIKMICRO-H10, Hikvision, China) to evaluate FA-FePt/DDP-NPs magnetothermal property in vivo. The treatment was repeated every 4 days. The size of the tumors was measured every 2 days and the tumors' volume was calculated as follows: volume=(length×width^2)/2. Four weeks later, the mice were killed, and the tumors and main organs were removed and the blood was collected. The volume and weight of tumors in each group were measured. The histological changes of tumor tissues were observed by HE staining. To evaluate the biosafety, the histology of the main organs including the heart, liver, spleen, lung, kidney, brain, and pancreas in the FA-FePt/DDP-NPs/MFH group was examined by HE staining and the biochemical indicators involved in bone marrow hematopoiesis such as peripheral blood leukocyte (WBC), red blood cell (RBC), hemoglobin, and platelet, and the indicators to assess liver and kidney function including alanine aminotransferase (ALT), aspartate aminotransferase (AST), urea nitrogen (BUN), creatinine (Cr), and total bilirubin (TBIL), in the mice serum before and after treatment were detected.

Statistical Analysis

Statistics software packages with SPSS 22.0 were used. Data have been presented as mean±SD. The comparison between the two groups was analyzed by *t*-test, and variance analysis was used for multiple comparisons. $p<0.05$ was considered statistically significant.

Results

Characterization of PEG-FePt-NPs and FA-PEG-FePt-NPs

Under TEM, the average particle size of FePt-NPs and PEG-FePt-NPs were both about 15 nm, uniform in size, and good in dispersion (Figure 1A). VSM detection showed FA-PEG-FePt-NPs had magnetic behavior (Figure 1B); XRD analysis showed the characteristic peaks of FePt (Figure 1C); energy dispersive X-ray (EDX) analysis showed the existence of C, O, Fe, and Pt, and their content of 6.95%, 1.60%, 3.52%, and 87.92%, respectively (Figure 1D). These results indicated FePt-NPs and PEG-FePt-NPs were successfully prepared.

Characterization of FA-PEG-FePt/DDP Nanoliposomes

The infrared spectra of FA-PEG-FePt-NPs, FePt-NPs, and folic acid (FA) are presented in Figure 2A. The emergence of new peaks and their precise positions could be distinctly discerned. Upon comparison with the FePt-NPs spectra, distinct characteristic peaks emerge in FA-PEG-FePt-NPs spectra which post-modification: one at 1727 cm^{-1}, attributable to the carboxyl group on PEG, and another at 1625 cm^{-1}, corresponding to the amide bond of DSPE-PEG. The distinct peaks observed in the spectrum confirmed the successful coating of PEG on the FePt-NPs' surface. Notably, a new peak at 1456.02 cm^{-1} was evident, which was solely attributed to the benzene ring presenting in FA. These results indicated FePt-NPs were successfully modified by PEG and coupled with FA. The size of the FA-FePt/DDP-NPs was verified about 30 nm by TEM, as depicted in Figure 2B. DLS revealed that the size of PEG-FePt-NPs ranged between 15 and 20 nm. This dimension subsequently increased to 70 nm following the process of liposome encapsulation and drug-loading. The observation over a duration of 0–140 hours indicated that the size of both PEG-FePt-NPs and FA-FePt/DDP-NPs was commendable in stability, as illustrated in Figure 2C. As delineated in the UV spectrum (Figure 2D), the distinctive absorption peak of DDP, situated around 300 nm, became apparent post-DDP loading. This observation signified the successful incorporation of DDP. An evaluation of the in vitro release of DDP from the nanoliposomes
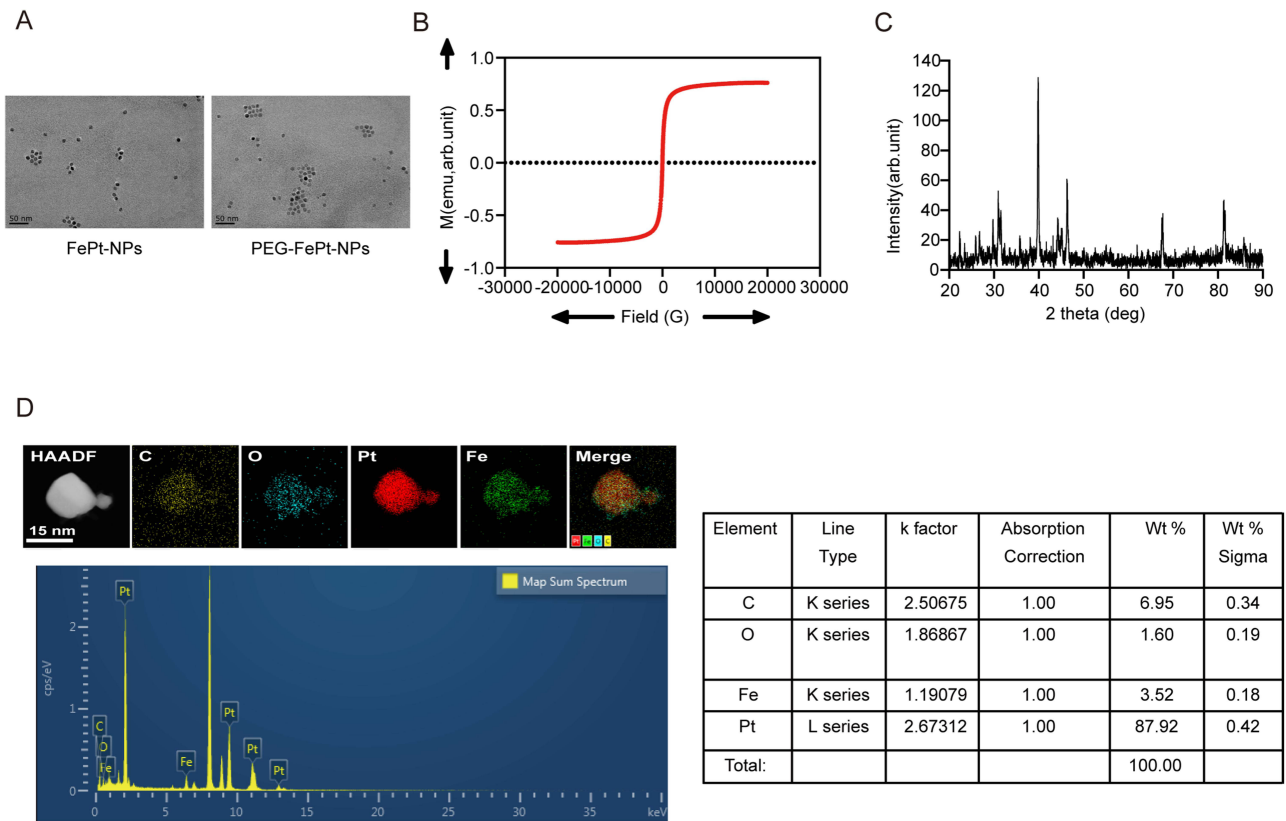
Figure 1 PEG-FePt-NPs characteristics. (**A**) The shape of FePt-NPs and PEG-FePt-NPs tested by TEM. (**B**) Vibrating sample magnetometry (VSM) result of PEG-FePt-NPs. (**C**) The structural characteristics of the FePt-NPs analyzed by X-ray diffraction (XRD). (**D**) The results of PEG-FePt-NPs analyzed by energy dispersive X-ray (EDX).
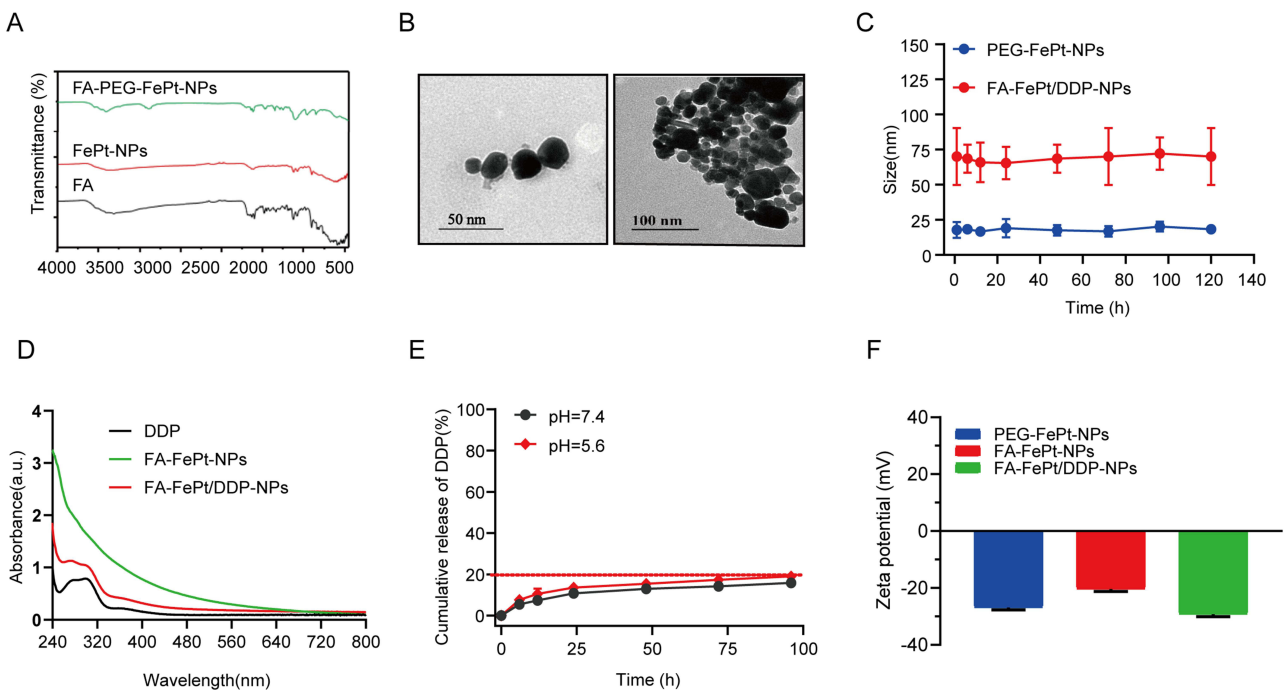

Figure 2 FA-FePt/DDP nanoliposomes characteristics. (**A**) Fluorescent intensity of the nanoparticles. (**B**) TEM images of FA-FePt/DDP nanoliposomes. (**C**) DLS of PEG-FePt-NPs and FA-FePt/DDP nanoliposomes. (**D**) UV spectrum after loading DDP. (**E**) DDP release from FA-FePt/DDP nanoliposomes in vitro. (**F**) Zeta potential of the nanoparticles.

was subsequently undertaken. The data indicate that the encapsulated DDP could slowly release, with the release ratio remaining under 20% in both acidic and neutral pH environments, as visualized in Figure 2E. Figure 2F shows a change in zeta potential from −29.37 mV to −21.73 mV, and finally to −30.62 mV in nanoparticles conjugated with the FA and DDP, respectively.

Cell Uptake and Biocompatibility Analysis

Although it has been reported that FR-α is overexpressed in ovarian cancer HO8910 cell line and not expressed in cervical cancer HeLa cell line, we further verified and confirmed it in our preliminary experiment (Figure S1). To detect the targeting and MRI potential of FA-PEG-FePt-NPs and FA-FePt/DDP-NPs, ovarian cancer cells (HO8910) and cervical cancer cells (HeLa) were thus selected as a model to observe cell-specific uptake capacity. Flow cytometry (Becton Dickinson, USA) was used to evaluate the internalization of NPs cells. As time went on, the fluorescence intensity of DID-labeled FA-FePt/DDP-NPs showed a strong fluorescence signal at 6 and 12 h and gradually amplified, accumulating efficiently in HO8910 cells. The cumulative amount at 12 h was higher than that at 6 h and 2 h. The cell uptake of FA-FePt/DDP-NPs increased with incubation time extending (Figure 3A and B). In high frequency alternating magnetic field with the frequency of 235 kHz, rated power 4 kW and voltage 40 A, PEG-FePt-NPs at different concentration could rise rapidly. The temperature of PEG-FePt-NPs (Fe: 1 mg/mL) and FA-FePt/DDP-NPs (Fe: 1 mg/mL) increased rapidly within 25 minutes, then maintained at 42–44 °C (Figure 3C and D). L-929 cells co-cultured with PEG-FePt-NPs grew well, and PEG-FePt-NPs at 0.25 mg/mL, 0.5 mg/mL, and 1 mg/mL within 36 h were all grade 1 in biosecurity, which met the requirements of medical biomaterials, while the cell proliferation rate of positive control group was only 16.8%, and its toxicity grade was grade 5, which was medically unqualified (Figure 3E). The hemolysis rate of PEG-FePt-NPs and FA-FePt-NPs was 2.13% and 1.62%, respectively, both less than 5% shown in Figure 3F, which met the application standard of medical biomaterials (ISO10993).

In vitro MRI Analysis of PEG-FePt-NPs, FA-PEG-FePt-NPs, and FA-PEG-FePt/DDP Nanoliposomes

After running the T2WI sequence scan of PEG-FePt-NPs at different concentration using Siemens 3.0T NMR, it was observed a stepwise decrease in T2 signal with the increase of PEG-FePt-NPs concentration (Figure 4A) at a relativity of 93.6 $mM^{-1}s^{-1}$
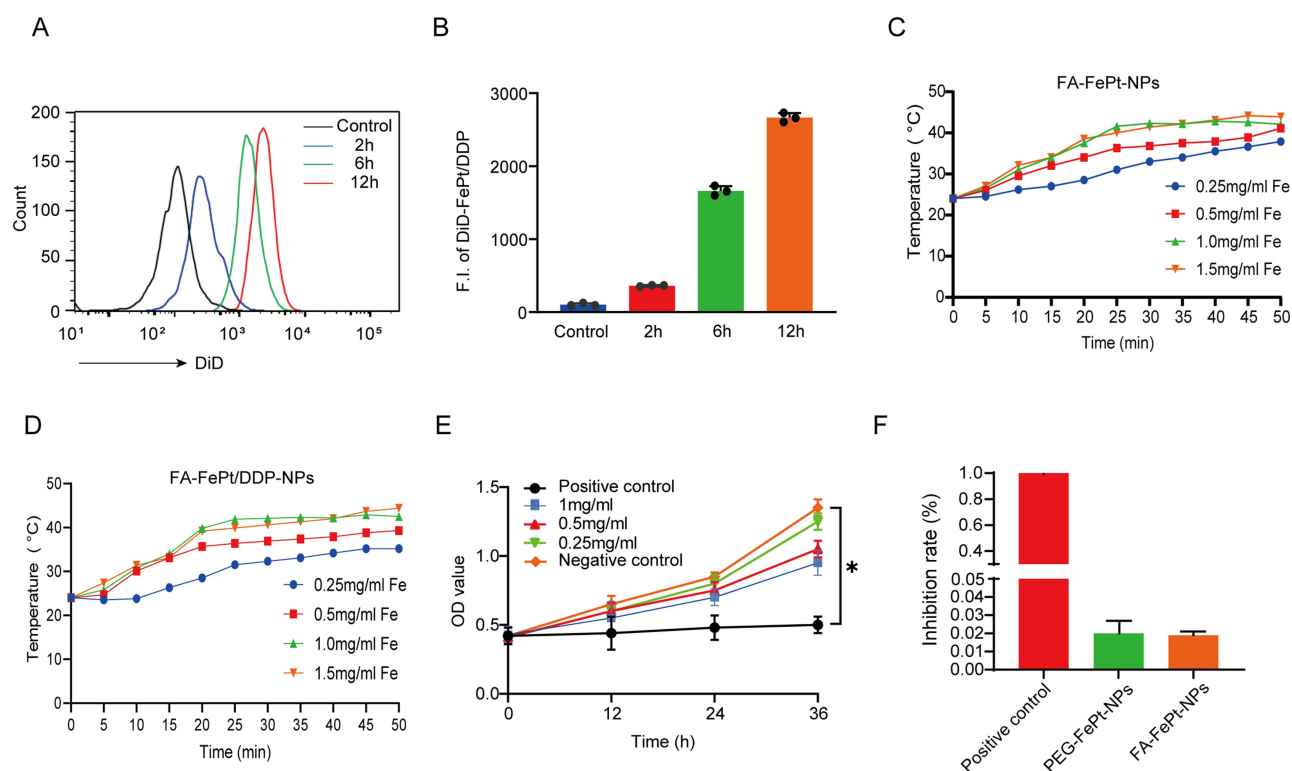

Figure 3 Cell uptake and biocompatibility analysis. (**A, B**) The cellular uptake of NPs was evaluated by flow cytometry. (**C, D**) In vitro magnetic induction heating curve of PEG-FePt-NPs and FA-FePt/DDP-NPs with different concentrations. (**E**) MTT experimental results of PEG-FePt-NPs. (**F**) Hemolysis rate of PEG-FePt-NPs and FA-PEG-FePt-NPs. *$p<0.05$.
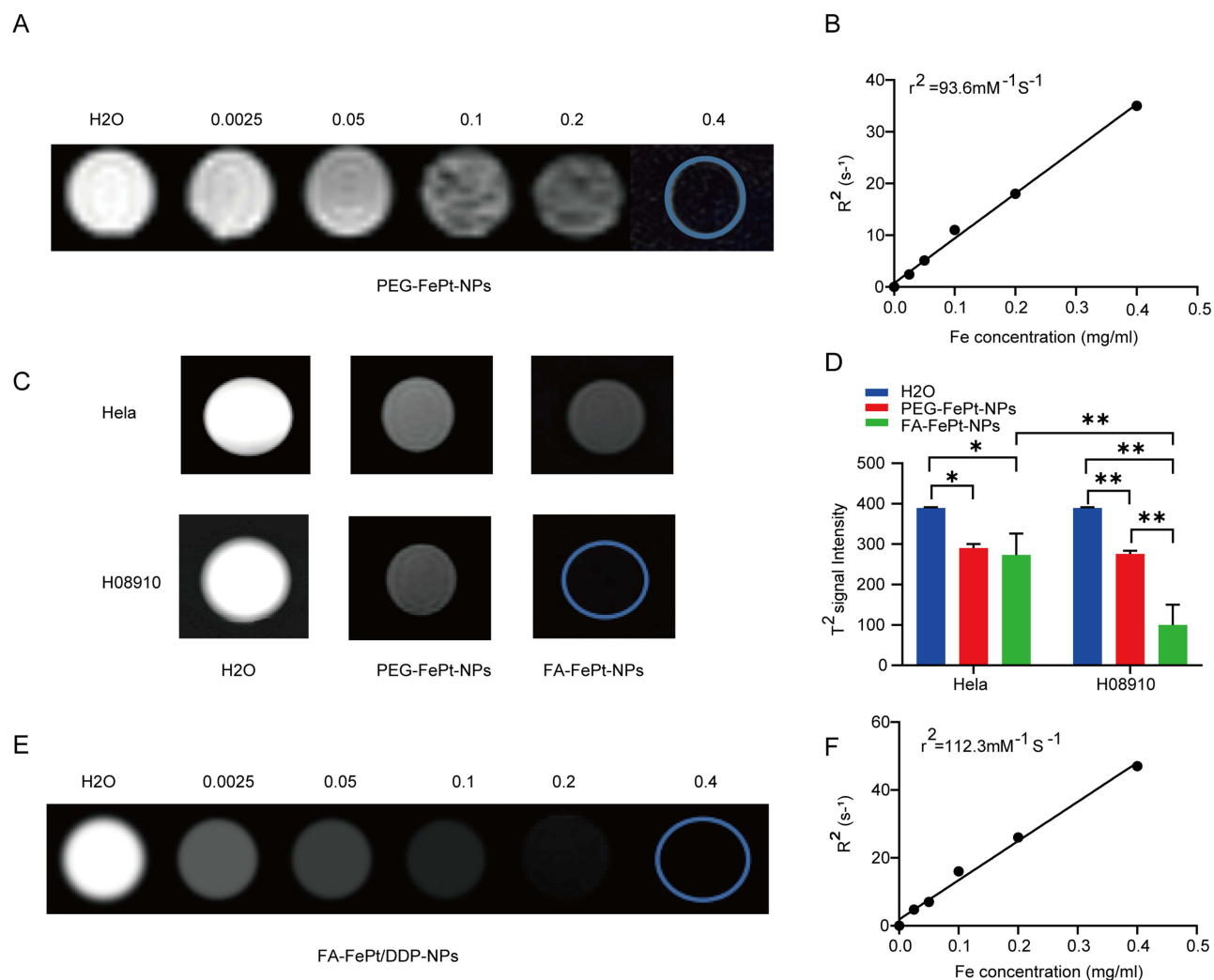
A

B

C

D

E

F

Figure 4 MRI study of PEG-FePt-NPs, FA-PEG-FePt-NPs, and FA-FePt/DDP nanoliposomes in vitro. (**A**) MR images of PEG-FePt-NPs with different concentrations of Fe (mg/mL). (**B**) Transverse relaxation time (R^2) of PEG-FePt-NPs. (**C, D**) T2 signal of PEG-FePt-NPs and FA-FePt-NPs after co-incubation with H08910 and HeLa cells. (**E**) T2-WI images obtained after MR imaging of FA-FePt/DDP-NPs with different concentrations. (**F**) The lateral relaxation time (R^2) of FA-FePt/DDP-NPs. *$p<0.05$, **$p<0.01$.

(Figure 4B), indicating good magnetic resonance imaging potential of PEG-FePt NPs. To further observe the molecular MRI of FA-FePt-NPs, ovarian cancer HO8910 cells and cervical cancer HeLa cells were respectively incubated with FA-FePt-NPs, and then washed and scanned by MR, in comparison with PEG-FePt-NPs. The results showed that both PEG-FePt-NPs and FA-FePt-NPs could inhibit the T2 signal of HO8910 cells and HeLa cells (Figure 4C and D), but the signal inhibitory of FA-FePt-NPs on HO8910 cells was significantly stronger than that on HeLa cells, and the inhibitory signal effect of FA-FePt-NPs on HO8910 cells was stronger than that of PEG-FePt-NPs. T2 signal inhibition effect on HeLa cell had no significant difference in FA-FePt-NPs and PEG-FePt-NPs. Figure 4E shows the images after magnetic resonance T2WI sequence scanning of FA-FePt/DDP-NPs at different concentrations. The T2 signal decreased step by step with the increase of FA-FePt/DDP nanoliposomes concentration, and its reflexivity was 112.3 mM^{-1}s^{-1} (Figure 4F), indicating that FA-FePt/DDP-NPs resulted from FePt/DDP-NPs coupled with FA still had a good magnetic resonance imaging potential.

Effects of FA-FePt/DDP Nanoliposomes on Proliferation, Apoptosis, and Epithelial Interstitial Transition of Ovarian Cancer HO8910 Cells in vitro

After intervention, the cell proliferation inhibitory in each group was examined. As shown in Figure 5A, the cell proliferation inhibition rate of FA-FePt/DDP-NPs/MFH group was (79.69 ±2.24)%, significantly higher than that of the PEG-FePt-NPs/MFH group (30.47±1.46)%, DDP group (51.76±4.57)% and FA-FePt-NPs/MFH group (52.23±1.29)%.
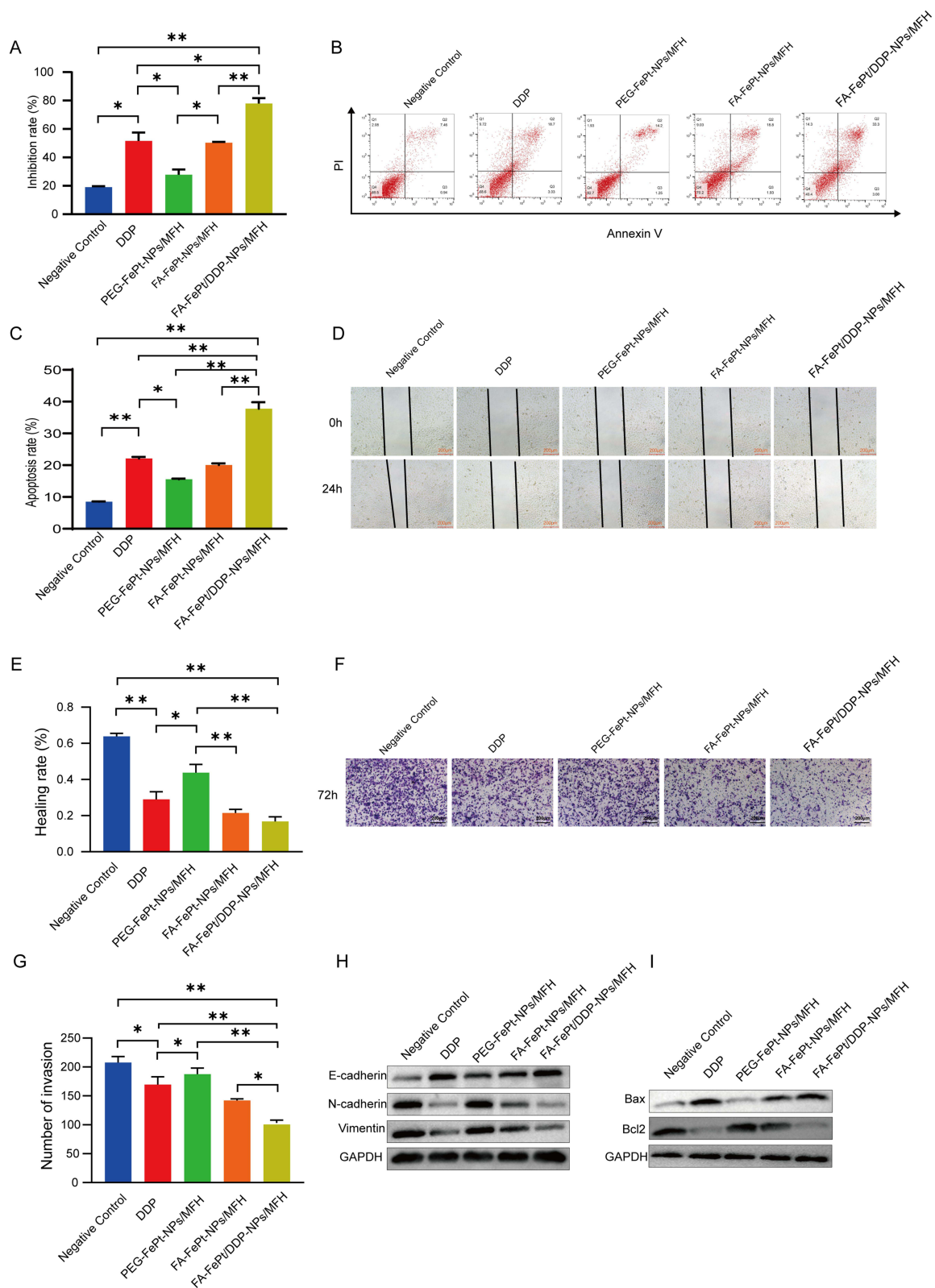
Figure 5 Effects of FA-FePt/DDP-NPs on migration, invasion, and apoptosis of HO8910 ovarian cancer cells in vitro. (**A**) Cell inhibition rate of each group. (**B, C**) Cell apoptosis of each group analyzed by flow cytometry. (**D, E**) Wound healing of each group. (**F, G**) Transwell of each group. (**H, I**) Protein expressions of different groups by WB assay. *$p<0.05$, **$p<0.01$.

The flow cytometry analysis showed that, in comparison with 8.5% of the control group, 21.73% of the DDP group, 15.45% of the PEG-FePt-NPs/MFH group, 20.43% of the FA-FePt-NPs/MFH group, the apoptosis rate of the FA-FePt/DDP-NPs/MFH group got to 36.3% (Figure 5B and C). The effects of FA-FePt/DDP-NPs in AMF on migration and invasion of HO8910 cells were examined by wound healing and transwell assays. As shown in Figure 5D–G, the cell migration and invasion inhibition of each treatment group was significantly higher than that of the negative control group (p<0.05), and the FA-FePt/DDP-NPs/MFH group showed the best effect, significantly lower than that of the other groups. The expression of proteins associated with EMT and apoptosis was detected by WB. E-cadherin protein and Bax expression were significantly up-regulated in FA-FePt/DDP-NPs/MFH group, while N-cadherin and Vimentin protein and Bcl-2 expression were significantly down-regulated (Figure 5H and I, Figure S2).

The Effects of FA-FePt/DDP Nanoliposomes in AMF on Ovarian Cancer Xenograft Tumor Growth in vivo

The effects of FA-FePt/DDP-NPs on ovarian cancer growth in vivo had been evaluated using a xenograft tumor model. The in vivo magnetothermal property of FA-FePt/DDP-NPs in AMF was verified by infrared thermal imagers. As shown in Figure 6A and B and Table S1, after exposure to AMF, the temperature around the tumor started to increase and then maintained at 43 °C or so after 20 minutes, and the heating range increased with time extension, while the control group has no magnetic thermal reaction. As shown in Figure 6C–F, compared with the negative control group, the tumor growth was inhibited in all treatment groups, but the FA-FePt/DDP-NPs/MFH group was the most significantly inhibited than the other groups. The tumor weight decreased in all treatment groups; based on tumor weight, we calculated tumor volume suppression rates of (42.43±1.37)%, (21.04±2.46)%, (63.07±3.24)%, and (72.02 ±2.84)% in different treatment groups (DDP, PEG-FePt-NPs/MFH, FA-FePt-NPs/MFH, and FA-FePt/DDP-NPs/MFH) respectively, especially in the FA-FePt/DDP-NPs/MFH group (p<0.05), while there was no significant difference in the weight of mice among five groups. HE staining showed that there was tumor tissue necrosis at different degree in each group, whereas the severest was in the FA-FePt/DDP-NPs/MFH group, with large necrotic area accompanied by tumor cell coagulation necrosis and nucleolysis. The immunohistochemical results showed that E-cadherin protein was significantly increased in the FA-FePt/DDP-NPs/MFH group, while N-cadherin and Vimentin proteins were significantly decreased. Bax expression was increased in all treatment groups, especially in the FA-FePt/DDP-NPs/MFH group, while Bcl-2 expression was reversed (Figure 6G).

In addition, we evaluated the biosafety in vivo of the FA-FePt/DDP-NPs/MFH group by blood routine detection [white blood cells (WBC), red blood cells (RBC), hemoglobin, and platelet], serum biochemical analysis [serum alanine aminotransferase (ALT), aspartate aminotransferase (AST), alkaline phosphatase (ALP), total bilirubin (TBIL), urea nitrogen (BUN), and creatinine (Cr)] and main viscerases' histopathological examination (heart, liver, spleen, lung, kidney, and pancreas). After treatment of FA-FePt/DDP-NPs in AMF, WBC of peripheral blood of tumor-bearing nude mice was $(5.08\pm0.40)\times10^9$/L. RBC was $(4.90\pm0.41)\times10^{12}$/L; Hb was (123.23 ± 13.35) g/L; platelet was $(240.56 \pm50.15)\times10^9$/L, and the blood counts and Hb concentration were all within the corresponding reference, indicating that there was no obvious adverse effect on bone marrow hematopoiesis. Similarly, serum ALT of FA-FePt/DDP-NPs with MFH group was (38.98 ± 3.63) U/L tumor bearing nude mice; AST was (132.93 ± 10.03) U/L; ALP was (137.81 ± 10.72) U/L; TBIL was (5.50 ± 0.22) μmol/L; BUN was (5.85 ± 0.40) mmol/L; and Cr was (5.65 ± 0.51) μmol/L. These results showed negligible differences in blood cells and serum biochemistry among all mice (Figure 7A–J) and no damage to the visceras (Figure 7K).

Discussion

Metal nanoparticles are a kind of material with wide application value.[32] As a promising tool in nanomedicine, MNPs have great potential in the diagnosis and treatment of various diseases.[33,34] Especially, FePt nanoparticles displayed a good prospect in cancer theranostics study in the past years. Except the general characteristic of nanomaterials such as small particle size and surface effect, etc., FePt nanoparticles own superparamagnetism, modifiable surface, good biocompatibility, high stability, easy synthesis and magnetocaloric effect, and non-immunogenicity, and they thus can be coupled with biological targeting molecules, anticancer drugs to realize their multi-functionalization.[35]
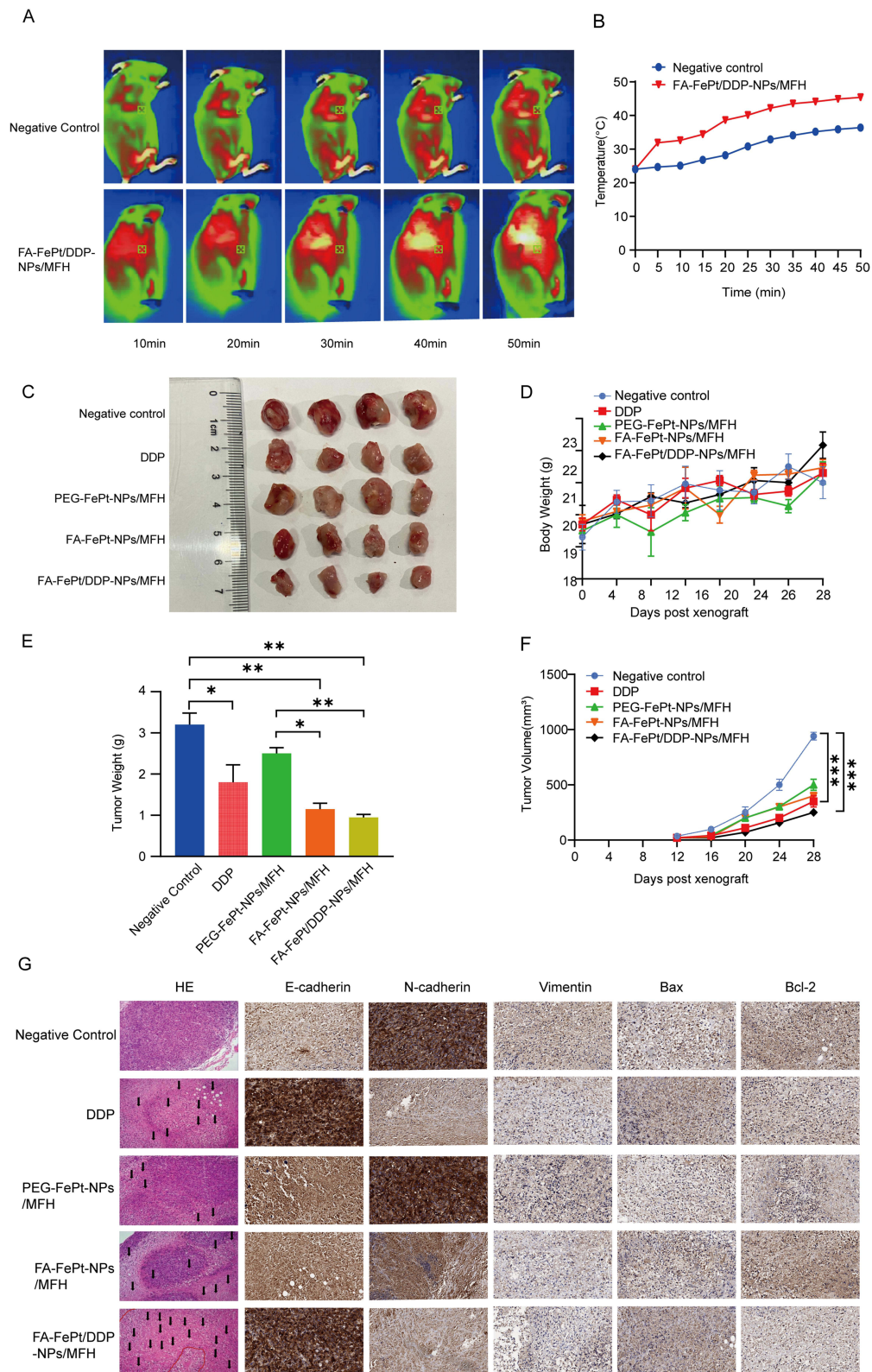
Figure 6 The therapeutic effects on ovarian cancer of different groups in vivo. (**A, B**) Mouse infrared thermal imaging. (**C**) Tumor gross samples. (**D**) Body weight change of mice as time. (**E**) Tumor weight change by group. (**F**) Tumor volume change as time. (**G**) The results of HE and IHC (black arrows point to tissue necrosis). *$p<0.05$, **$p<0.01$, ***$p<0.001$.
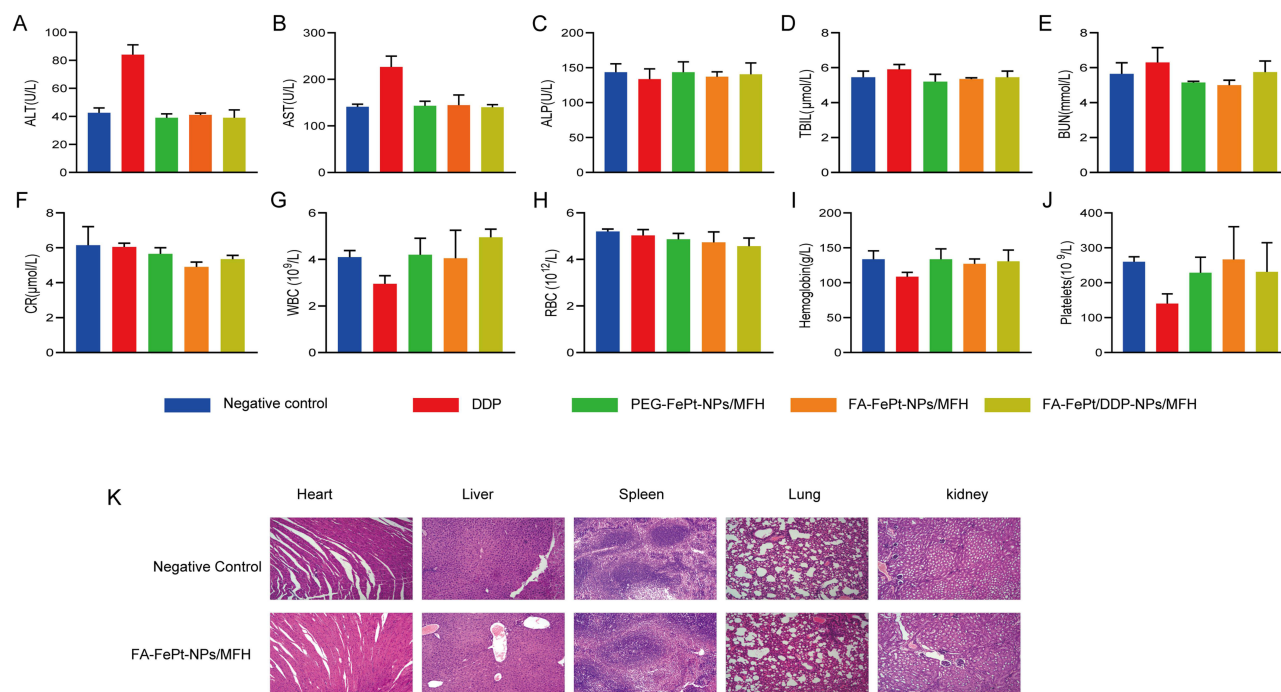
Figure 7 Adverse effect examination of different groups (WBC, RBC, hemoglobin and platelet, and ALT, AST, ALP, BUN, Cr, TBIL). (**A–J**) Detection of serum biochemical indicators and blood cells in each group. (**K**) Histopathological examination of main visceras.

However, since magnetic nanoparticles may be taken in by the reticuloendothelial system in the blood circulation, fewer particles can reach lesion and they need to satisfy certain size requirements when used in biomedical field. As a rule, when the particle size is small enough (<100 nm), the uptake process of nanoparticles by the reticuloendothelial system is delayed and can effectively reach the focusing area under the action of external magnetic field.[36] In the present study, FePt-NPs were successfully prepared by high temperature liquid phase reduction method and then surface modified with PEG. Then FA was coupled with and DDP was encapsulated in, eventually, PEG-FePt-NPs, FA-FePt-NPs, and FA-FePt/DDP-NPs were obtained. The average size of FePt-NPs and PEG-FePt-NPs both were about 15 nm with good magnetic responsiveness, no hemolysis and cytotoxicity. FA-FePt-NPs were about 30 nm in diameter and FA-FePt/DDP-NPs were about 70 nm in hydrated particle size. The infrared spectra indicated FA was coupled and DDP was loaded to PEG-FePt-NPs.

In AMF, PEG-FePt-NPs in vitro and tumor tissue with FA-FePt/DDP-NPs in vivo both were rapidly warmed in 25 min, and then maintained at 42–44 °C. This is an ideal temperature to treat tumor since cancer cells are generally more sensitive to heat than normal cells within this temperature range because of cancer cell incomplete membrane structure and specific tumor microenvironment. In detail, the critical temperature leading to death for most tumor cells is 42–43.5 °C, whereas normal cells are not sensitive to this temperature; tumor cells cannot be effectively killed at less 42 °C. When temperature is over 42 °C, thermal damage becomes obviously, and killed cancer cells in quantity can double when temperature rise by 1 °C. But when it is more than 45 °C, tumor tissue and normal tissue has no difference in the thermal sensitivity, signifying damage on normal tissue.[37]

As a currently extensively applied noninvasive medical diagnostic technique, MRI has many indications and exerts an important role in the early detection and diagnosis of cancer.[38] At present, the contrast agents used in MRI are mainly divided into two categories: inhibition of T1 (such as paramagnetic metal ions Gd^{3+} and Mn^{2+}) and inhibition of T2 (including superparamagnetism and ferromagnetic substances).[39] Superparamagnetic iron-based nanoparticles were widely studied in the field of MRI, for example, Fe_3O_4 nanoparticles were reported to be well applied as contrast developers for T2-weighted MRI images.[40] In the current work, PEG-FePt-NPs we prepared effectively suppressed the signal intensity of T2 image in MRI. Their transverse relaxation time (r^2) was calculated as 93.6 $mM^{-1}s^{-1}$, implying a superior potential for magnetic resonance imaging. Moreover, FA-FePt-NPs and PEG-FePt-NPs incubated with ovarian

cancer HO8910 cells (FR-α^+) suppressed the T2 signal on T2WI images in comparison with the control, whereas FA-FePt-NPs exerted a more potent inhibition than PEG-FePt-NPs did, but there was no significant difference in T2 signal of HeLa cell groups (FR-α^-). Besides, FA-FePt-NPs had an increased effect on suppressing T2 signal in the HO8910 cell group compared with that in the HeLa cell group. This may be a result of the specific role of FA-FePt-NPs in tumor cells with FR overexpressed. In addition, flow cytometry detection also showed a good uptake and internalization of DID-labeled FA-FePt/DDP-NPs by HO8910 cells, and FA-FePt/DDP-NPs also could inhibit the T2 signal when exerting T2WI sequence scanning, showing a good magnetic resonance imaging potential. Moreover, these results also signified a good targeting of FA-FePt-NPs and FA-FePt/DDP-NPs to ovarian cancer with overexpressed FR-α. It is thus speculated that FA-FePt-NPs have a good potential using as a novel molecular probe of MRI, but this need further investigation in vitro and in vivo.

Thermotherapy can directly induce cancer cell death via heating, and may also exert a synergistic effect on radiotherapy, surgery, immunotherapy, and chemotherapy.[19,41] The results of our previous study suggested FePt-NPs had a property to generate heat in AMF.[42] In the present work, we prepared FA-FePt/DDP-NPs and integrated folate receptor-targeting DDP and MFH to intervene ovarian cancer. As a result, ovarian cancer cells were significantly inhibited in proliferation, migration, and invasion and induced to apoptosis in vitro. The in vivo experiment showed that the tumor weight and size obviously decreased after the intervention of FA-FePt/DDP-NPs combined with MFH, with a good therapeutic effect on ovarian cancer.

To further investigate the therapeutic effects in molecular level, we detected the expression of the genes related to apoptosis (Bax and Bcl-2) and EMT (E-cadherin, N-cadherin, and Vimentin) by WB and immunohistochemical analysis in vivo and in vitro. EMT refers to the process of transforming epithelial cells into stromal cells and gaining the ability of invasion and migration.[43] This process depends on the downregulation of E-cadherin epithelial markers and the upregulation of N-cadherin and Vimentin mesenchymal markers. As a rule, the loss of E-cadherin is considered to be a typical feature of EMT.[44] The expression of E-cadherin is regulated by various transcription factors, including Snail, Slug, Twist, ZEB1, and ZEB2. N-cadherin is a classic member of the calcium-binding protein family. It has been reported by Heuberger et al[45] that N-cadherin expression upregulation contributed to angiogenesis and EMT, making tumor cells more invasive and prone to metastasis. Vimentin, an important protein for maintaining cell integrity, is frequently reported in various epithelial cancers with malignant transformation, including prostate cancer, breast cancer, malignant melanoma, and other types of cancer.[46] The molecular investigation in this study showed FA-FePt/DDP-NPs in AMF inhibited the tumor growth, invasion, and migration by up-regulating E-cadherin and down-regulating N-cadherin and Vimentin protein, and simultaneously promoted tumor cells apoptosis by Bax protein up-regulation and Bcl-2 protein down-regulation.

In biosafety, it was shown no toxic side effects after the treatment of FA-FePt/DDP-NPs combined with MFH. In detail, serum biochemical detection suggested no damage to liver and kidney function, and blood cell examination showed no inhibition effect on myelopoiesis. The histopathological examination presented no pathological changes in visceras including the heart, liver, spleen, lung, kidney, and pancreas.

Taken together, this study provided a new idea of integrated targeting therapy and diagnosis for ovarian cancer, but this needs to be further investigated in the subsequent studies in vitro and in vivo. For example, ovarian cancer cells may be injected with intraperitoneal injection (IP) to construct a mouse model of diffuse small tumor common in clinical ovarian cancer. Magnetic targeted nanomedicine will be tried injecting by tail vein to observe the inhibition of magnetic resonance signals at the tumor location and analyze the enrichment of materials at the tumor location. This will better support imaging and therapy study of the nanoparticles in mice.

Conclusion

In conclusion, FA-FePt-NPs and FA-PEG-FePt/DDP nanoliposomes were successfully synthesized. It was confirmed that FA-FePt-NPs could specifically target to cancer cells with overexpressed FR and may be a candidate contrast agent for molecular magnetic resonance to detect ovarian cancer. FA-FePt/DDP-NPs also showed a potential of MRI, and FA-FePt/DDP-NPs in AMF could effectively inhibit the malignant progress of ovarian cancer by suppressing tumor cell proliferation, invasion, and migration and inducing tumor cell apoptosis, with no obvious adverse effect. Therefore, FA-

FePt/DDP-NPs combined with MFH may be used for an integration of targeted thermo-chemotherapy and diagnosis for ovarian cancer guided by MRI.

Acknowledgments

Disclosure

The authors declare no conflicts of interest in this work.

References

1. Zuo K, Zhao Y, Zheng Y, et al. Long non-coding RNA XIST promotes malignant behavior of epithelial ovarian cancer. *Onco Targets Ther*. 2019;12:7261–7267. doi:10.2147/OTT.S204369
2. Zhang Y, Dun Y, Zhou S, et al. LncRNA HOXD-AS1 promotes epithelial ovarian cancer cells proliferation and invasion by targeting miR-133a-3p and activating Wnt/β-catenin signaling pathway. *Biomed Pharmacother*. 2017;96:1216–1221. doi:10.1016/j.biopha.2017.11.096
3. Bocchicchio S, Tesone M, Irusta G, et al. Convergence of Wnt and Notch signaling controls ovarian cancer cell survival. *J Cell Physiol*. 2019;234 (12):22130–22143. doi:10.1002/jcp.28775
4. Liang X, Guo W, Ren T, et al. Macrophages reduce the sensitivity of osteosarcoma to neoadjuvant chemotherapy drugs by secreting Interleukin-1 beta. *Cancer Lett*. 2020;480:4–14. doi:10.1016/j.canlet.2020.03.019
5. WS JX, Parkinson DY, Yi MYJ, et al. 3D printed absorber for capturing chemotherapy drugs before they spread through the body. *ACS Cent Sci*. 2019;5(3):419–427. doi:10.1021/acscentsci.8b00700
6. Wang T, Zhou Y, Lei C, Luo J, Xie S, Pu H. Magnetic impedance biosensor: a review. *Biosens Bioelectron*. 2017;90:418–435. doi:10.1016/j. bios.2016.10.031
7. Taheri-Ledari R, Zhang W, Radmanesh M, et al. Multi-stimuli nanocomposite therapeutic: docetaxel targeted delivery and synergies in treatment of human breast cancer tumor. *Small*. 2020;16(41):e2002733. doi:10.1002/smll.202002733
8. Taheri-Ledari R, Zolfaghari E, Zarei-Shokat S, Kashtiaray A, Maleki A. A magnetic antibody-conjugated nano-system for selective delivery of Ca(OH)2 and taxotere in ovarian cancer cells. *Commun Biol*. 2022;5(1):995. doi:10.1038/s42003-022-03966-w
9. Taheri-Ledari R, Tarinsun N, Sadat Qazi F, et al. Vancomycin-Loaded Fe3O4/MOF-199 Core/Shell Cargo Encapsulated by Guanidylated-β-Cyclodextrine: An effective antimicrobial nanotherapeutic. *Inorg Chem*. 2023;62(6):2530–2547. doi:10.1021/acs.inorgchem.2c02634
10. Mohaghegh S, Tarighatnia A, Omidi Y, et al. Multifunctional magnetic nanoparticles for MRI-guided co-delivery of erlotinib and L-asparaginase to ovarian cancer. *J Microencapsul*. 2022;39(4):394–408. doi:10.1080/02652048.2022.2094487
11. Amraee A, Khoei S, Mahdavi SR, et al. Ultrasmall iron oxide nanoparticles and gadolinium-based contrast agents in magnetic resonance imaging: a systematic review and meta-analysis. *Clin Transl Imaging*. 2023;11:83–93. doi:10.1007/s40336-022-00528-2
12. Foroughi-Nia B, Aghanejad A, Kadkhoda J, Barar J, Nosrati H, Davaran S. AS1411 conjugated magnetic-based poly N-isopropyl acrylamide nanoparticles for delivery of erlotinib to prostate cancer cells. *Appl Organomet Chem*. 2022;36(7):e6691. doi:10.1002/aoc.6691
13. Wu L, Mendoza-Garcia A, Li Q, Sun S. Organic phase syntheses of magnetic nanoparticles and their applications. *Chem Rev*. 2016;116 (18):10473–10512. doi:10.1021/acs.chemrev.5b00687
14. Chen B, Sun J, Fan F, et al. Ferumoxytol of ultrahigh magnetization produced by hydrocooling and magnetically internal heating co-precipitation. *Nanoscale*. 2018;10(16):7369–7376. doi:10.1039/c8nr00736e
15. Huynh KH, Pham XH, Kim J, et al. Synthesis, Properties, and Biological Applications of Metallic Alloy Nanoparticles. *Int J Mol Sci*. 2020;21 (14):5174. doi:10.3390/ijms21145174
16. Kim J, Cho HR, Jeon H, et al. Continuous O2-Evolving MnFe2O4 Nanoparticle-Anchored mesoporous silica nanoparticles for efficient photo-dynamic therapy in hypoxic cancer. *J Am Chem Soc*. 2017;139(32):10992–10995. doi:10.1021/jacs.7b05559
17. Hu H, Masarapu H, Gu Y, et al. physalis mottle virus-like nanoparticles for targeted cancer imaging. *ACS Appl Mater Interfaces*. 2019;11 (20):18213–18223. doi:10.1021/acsami.9b03956
18. Louie A. Multimodality imaging probes: design and challenges. *Chem Rev*. 2010;110(5):3146–3195. doi:10.1021/cr9003538
19. Zheng Y, Tang Y, Bao Z, et al. FePt nanoparticles as a potential X-ray activated chemotherapy agent for HeLa cells. *Int J Nanomed*. 2015;10:6435–6444. doi:10.2147/IJN.S88458
20. Skok K, Zidarič T, Orthaber K, et al. Novel Methacrylate-Based Multilayer Nanofilms with Incorporated FePt-Based Nanoparticles and the Anticancer Drug 5-Fluorouracil for Skin Cancer Treatment. *Pharmaceutics*. 2022;14(4):689. doi:10.3390/pharmaceutics14040689
21. Pratt EC, Shaffer TM, Grimm J. Nanoparticles and radiotracers: advances toward radionanomedicine. *Wiley Interdiscip Rev Nanomed Nanobiotech*. 2016;8(6):872–890. doi:10.1002/wnan.1402
22. Sun H, He S, Wen B, Jia W, Fan E, Zheng Y. Effect of Biejiajian Pills on Wnt signal pathway molecules β-catenin and GSK-3β and the target genes CD44v6 and VEGF in hepatocellular carcinoma cells. *Nan Fang Yi Ke Da Xue Xue Bao*. 2014;34(10):1454–1458.
23. Guohua H, Hongyang L, Zhiming J, et al. Study of small-cell lung cancer cell-based sensor and its applications in chemotherapy effects rapid evaluation for anticancer drugs. *Biosens Bioelectron*. 2017;97:184–195. doi:10.1016/j.bios.2017.05.050
24. Karampelias C, Rezanejad H, Rosko M, et al. Reinforcing one-carbon metabolism via folic acid/Folr1 promotes β-cell differentiation. *Nat Commun*. 2021;12(1):3362. doi:10.1038/s41467-021-23673-0

25. Morris RT, Joyrich RN, Naumann RW, et al. Phase II study of treatment of advanced ovarian cancer with folate-receptor-targeted therapeutic (vintafolide) and companion SPECT-based imaging agent (99mTc-etarfolatide). *Ann Oncol*. 2014;25(4):852–858. doi:10.1093/annonc/mdu024

26. Luiz MT, Tofani LB, Araújo VHS, et al. Gene therapy based on lipid nanoparticles as non-viral vectors for glioma treatment. *Curr Gene Ther*. 2021;21(5):452–463. doi:10.2174/1566523220999201230205126

27. Ulbrich K, Holá K, Šubr V, et al. Targeted Drug Delivery with Polymers and Magnetic Nanoparticles: covalent and Noncovalent Approaches, Release Control, and Clinical Studies. *Chem Rev*. 2016;116(9):5338–5431. doi:10.1021/acs.chemrev.5b00589

28. Liu Y, Yang F, Yuan C, et al. Magnetic Nanoliposomes as in Situ Microbubble Bombers for Multimodality Image-Guided Cancer Theranostics. *ACS Nano*. 2017;11(2):1509–1519. doi:10.1021/acsnano.6b06815

29. Mei L, Yan X. A Combination Therapy of pHRE-Egr1-HSV-TK/AntiCD133McAb-131I/MFH Mediated by FePt Nanoparticles for Liver Cancer Stem Cell. *J Nanomater*. 2020;2020:1–15.

30. USP XXII, NF XVII [S].United States Pharmacopeial Convention,Inc,1990; 2069.

31. Guo T, Zhu Y, Yue M, et al. The Therapeutic Effects of DDP/CD44-shRNA Nanoliposomes in AMF on Ovarian Cancer. *Front Oncol*. 2022;12:811783. doi:10.3389/fonc.2022.811783

32. Baran A, Baran MF, Keskin C. Ecofriendly/rapid synthesis of silver nanoparticles using extract of waste parts of artichoke (Cynara scolymus L.) and evaluation of their cytotoxic and antibacterial activities. *J Nanomater*. 2021;2021:1–10. doi:10.1155/2021/2270472

33. Niculaes D, Lak A, Anyfantis GC, et al. Asymmetric assembling of iron oxide nanocubes for improving magnetic hyperthermia performance. *ACS Nano*. 2017;11(12):12121–12133. doi:10.1021/acsnano.7b05182

34. Eftekhari A, Arjmand A, Asheghvatan A, et al. The potential application of magnetic nanoparticles for liver fibrosis theranostics. *Front Chem*. 2021;9:674786. doi:10.3389/fchem.2021.674786

35. Li X, Lu S, Xiong Z, et al. Light-Addressable Nanoclusters of Ultrasmall Iron Oxide Nanoparticles for enhanced and dynamic magnetic resonance imaging of arthritis. *Adv Sci*. 2019;6(19):1901800. doi:10.1002/advs.201901800

36. Meyer TA, Zhang C, Bao G, et al. Programmable Assembly of Iron Oxide Nanoparticles Using DNA Origami. *Nano Lett*. 2020;20(4):2799–2805. doi:10.1021/acs.nanolett.0c00484

37. Lin M, Huang J, Jiang X, et al. A combination hepatoma-targeted therapy based on nanotechnology: pHRE-Egr1-HSV-TK/(131)I-antiAFPMcAb-GCV/MFH. *Sci Rep*. 2016;6:33524. doi:10.1038/srep33524

38. Chabanova E, Larsen L, Løgager VB, Møller JM, Thomsen HS. Anvendelse af MR-scanning [Use of magnetic resonance imaging]. *Ugeskr Laeger*. 2014;176(1):50–54.

39. an R, Hossein A, Kheirjou S, Amoabediny G, Ardestani MS, Mohammadnejad J. Monodisperse magnetite (Fe3O4) nanoparticles modified with water soluble polymers for the diagnosis of breast cancer by MRI method. *J MAGNET MAGN MAT*. 2016;420(15):210–217. doi:10.1016/j.jmmm.2016.07.003

40. Slabu I, Wiemer K, Steitz J, et al. Size-Tailored Biocompatible FePt Nanoparticles for Dual T1/T2 magnetic resonance imaging contrast enhancement. *Langmuir*. 2019;35(32):10424–10434. doi:10.1021/acs.langmuir.9b00337

41. Neuwelt A, Sidhu N, Hu CA, et al. Iron-based superparamagnetic nanoparticle contrast agents for MRI of infection and inflammation. *AJR Am J Roentgenol*. 2015;204(3):W302–13. doi:10.2214/AJR.14.12733

42. Lin M, Xiao YH, Jiang XM, et al. A Combination Therapy of pHRE-Egr1-HSV-TK/Anti-CD133McAb-131 I/MFH Mediated by FePt nanoparticles for liver cancer stem cells. *J Nanomater*. 2020;1–15. doi:10.1155/2020/7180613.

43. Friend C, Parajuli P, Razzaque MS, et al. Deciphering epithelial-to-mesenchymal transition in pancreatic cancer. *Adv Cancer Res*. 2023;159:37–73. doi:10.1016/bs.acr.2023.02.008

44. Das V, Bhattacharya S, Chikkaputtaiah C, et al. The basics of epithelial-mesenchymal transition (EMT): a study from a structure, dynamics, and functional perspective. *J Cell Physiol*. 2019;234(9):14535–14555. doi:10.1002/jcp.28160

45. Heuberger J, Birchmeier W. Interplay of cadherin-mediated cell adhesion and canonical Wnt signaling. *Cold Spring Harb Perspect Biol*. 2010;2(2):a002915. doi:10.1101/cshperspect.a002915

46. Loh CY, Chai JY, Tang TF, et al. The E-Cadherin and N-Cadherin Switch in Epithelial-to-mesenchymal transition: signaling, therapeutic implications, and challenges. *Cells*. 2019;8(10):1118. doi:10.3390/cells8101118